

1 **Supporting Information for**  
 2 **“SERMeQ model produces realistic retreat of 155 Greenland out-**  
 3 **let glaciers”**

4 **Lizz Ultee<sup>1</sup> and Jeremy Bassis<sup>2</sup>**

5 <sup>1</sup>Department of Earth, Atmospheric, and Planetary Sciences, Massachusetts Institute of Technology,  
 6 Cambridge, MA, USA.

7 <sup>2</sup>Department of Climate & Space Sciences, University of Michigan, Ann Arbor, MI, USA.

8 **Contents**

- 9 1. Text S1 to S5  
 10 2. Figures S1 to S5

11 **Additional Supporting Information (Files uploaded separately)**

- 12 1. Table S1, a list of all Greenland outlet glaciers in the MEaSURES dataset with  
 13 their glacier ID number, name(s), optimal yield strength found, and notes on  
 14 inclusion in the analysis. The note “Flagged for bad flowline trace” indicates  
 15 glaciers that required manual intervention to complete data processing, but  
 16 which are now included in the analysis.

17 **Introduction**

18 **Text S1. Ice dynamics in SERMeQ**

The ice dynamics in our model are based on a perfectly-plastic limiting case of a viscoplastic rheology (Bassis & Ultee, 2019). This rheology describes a glacier with two characteristic timescales: viscous deformation (slow) and mass loss by calving (fast). Modifications to the simple plastic formulation allow calving at a grounded ice-water interface (Ultee & Bassis, 2016) and interaction between multiple tributary glaciers (Ultee & Bassis, 2017). By requiring instantaneous stress balance across the glacier terminus, this formulation finds that the ice thickness  $H_{\text{terminus}}$  at a given terminus position, in water of depth  $D$ , is limited by the yield strength and cannot exceed

$$H_{\text{terminus}} = 2 \frac{\tau_y}{\rho_i g} + \sqrt{\frac{\rho_w}{\rho_i} D^2 + 2 \frac{\tau_y}{\rho_i g}}, \quad (\text{S1})$$

19 with  $\tau_y$  the yield strength of glacier ice,  $\rho_i = 920 \text{ kg m}^{-3}$  the density of glacier ice,  
 20  $\rho_w = 1020 \text{ kg m}^{-3}$  the density of seawater, and  $g = 9.81 \text{ m s}^{-2}$  the acceleration due  
 21 to gravity (Ultee & Bassis, 2016).

In a perfectly plastic glacier (Nye, 1951), the upstream ice thickness  $H$  along a central flowline, with along-flow direction  $x$  and ice surface elevation  $s$ , is also controlled by the yield strength:

$$H \frac{\partial s}{\partial x} = \frac{\tau_y}{\rho_i g}. \quad (\text{S2})$$

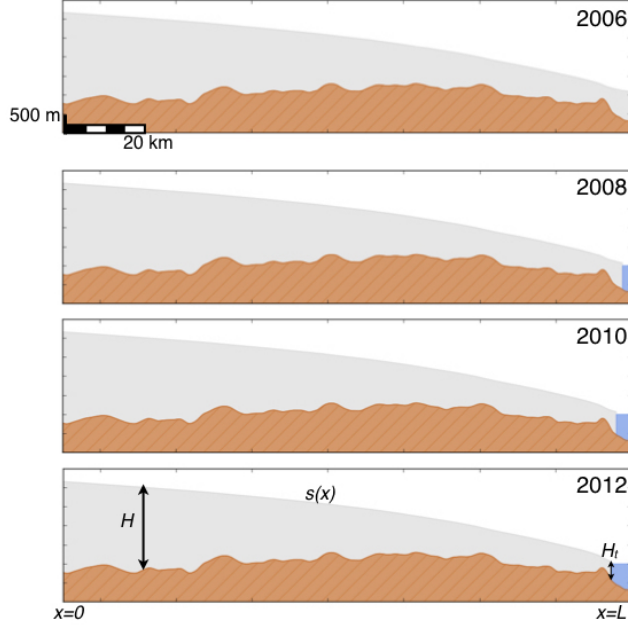
22 This approximation corresponds to a case where the glacier bed is (nearly) plastic  
 23 and the glacier stress balance is dominated by shear at the glacier bed and valley  
 24 walls—appropriate for most Greenland outlet glaciers. We also account for longitudinal

---

Corresponding author: L. Ultee, [ehultee@umich.edu](mailto:ehultee@umich.edu)

25 stresses in a boundary layer near the terminus, where they are more likely to be  
 26 important (Bassis & Ultee, 2019).

27 Finally, we use mass continuity to derive an expression for the rate of terminus  
 28 advance or retreat due to calving (see Text S2, below). With each change in terminus  
 29 position, we calculate a new surface profile according to Equations S1-S2. Figure S1  
 30 shows an example sequence of glacier profiles as calculated by SERMeQ.



31 **Figure S1.** Surface profiles produced by SERMeQ along a flowline in the central part of  
 32 Sermeq Kujalleq’s catchment. Profiles show glacier ice in grey, bedrock in brown, and fjord wa-  
 33 ter in blue. Spatial scale is indicated on the first panel and consistent throughout. Labels on  
 34 lower panel indicate along-flow direction  $x$ , ice surface elevation  $s(x)$ , ice thickness  $H$ , terminus  
 35 ice thickness  $H_t$ , and terminus location  $x = L$  as used in Equations S1-S6. For comparison of  
 36 observed versus simulated surface profiles, see Ultee and Bassis (2016, 2017).

37 Despite the simplicity of the model, preliminary experiments have shown promise  
 38 in reproducing both surface elevation profiles and advance/retreat rates of glaciers in  
 39 Alaska and Greenland (Ultee & Bassis, 2016, 2017). However, our model only applies to  
 40 grounded glaciers and cannot simulate the dynamics of floating ice tongues or shelves.

41 **Text S2. Time evolution of the terminus position**

42 Glacier terminus position in SERMeQ evolves in response to near-terminus stretch-  
 43 ing, bedrock topography, and changes in catchment-wide surface mass balance as  
 44 described in Ultee (2018) and Bassis and Ultee (2019). Below is a brief summary  
 45 derivation of the terminus evolution condition as implemented in SERMeQ code.

46 Let  $x = 0$  represent the ice divide and  $x = L$  the terminus, where  $L = L(t)$  is the  
 47 length of the glacier (labelled in Figure S1). The time derivative  $dL/dt$  then represents  
 48 the change in terminus position over time.

Taking the material derivative of the terminus ice thickness  $H = H_y$  (constrained by Equation S1), we find

$$\begin{aligned} \left. \frac{DH}{Dt} \right|_{x=L} &= \frac{DH_y}{Dt} \\ \left[ \frac{\partial H}{\partial t} + \frac{dL}{dt} \frac{\partial H}{\partial x} \right]_{x=L} &= \frac{\partial H_y}{\partial t} + \frac{dL}{dt} \frac{\partial H_y}{\partial x} \\ \left. \frac{\partial H}{\partial t} \right|_{x=L} &= \frac{dL}{dt} \left[ \frac{\partial H_y}{\partial x} - \frac{\partial H}{\partial x} \right]_{x=L}. \end{aligned} \quad (\text{S3})$$

Mass continuity requires

$$\frac{\partial H}{\partial t} + \frac{\partial}{\partial x}(HU) = \dot{a} \quad (\text{S4})$$

49 where  $H = H(x, t)$  is the ice thickness,  $U = U(x, t)$  the ice velocity, and  $\dot{a} = \dot{a}(x, t)$   
50 the net ice accumulation rate, for all  $(x, t)$ .

Substituting equation (S4) into (S3), we find

$$\dot{a} - H \frac{\partial U}{\partial x} - U \frac{\partial H}{\partial x} = \frac{dL}{dt} \left[ \frac{\partial H_y}{\partial x} - \frac{\partial H}{\partial x} \right]_{x=L} \quad (\text{S5})$$

$$\frac{dL}{dt} = \frac{\dot{a} - H \frac{\partial U}{\partial x} - U \frac{\partial H}{\partial x}}{\frac{\partial H_y}{\partial x} - \frac{\partial H}{\partial x}}, \quad (\text{S6})$$

51 with all terms of equation (S6) evaluated at  $x = L$ , the terminus of the glacier (compare  
52 with Equation 54 of Bassis and Ultee (2019)). With the exception of ice accumulation  
53 rate  $\dot{a}$ , all terms are determined by the rheology of ice.

Upstream from the terminus, we assume a plastic yielding layer at the bed of the glacier. A perfectly plastic glacier would have a rigid ice plug above the yielding layer, but the perfect plastic approximation is a limiting case of several other rheologies that could be used to describe the slow deformation of ice in a pseudo-plug (e.g. Balmforth et al., 2006). Here we choose to describe the slow deformation of intact ice with the familiar Glen's flow law. At the terminus, as in Ultee and Bassis (2016, 2017), we require a vertical yield surface to describe the more rapid motion of fractured, disarticulated ice as it calves away from the intact glacier. This implies that the effective stress in a region of length  $\delta$  upstream from the terminus is within  $\epsilon$  of the yield strength  $\tau_y$ . Near the terminus, we have

$$\begin{aligned} \frac{\partial U}{\partial x} &= \dot{\epsilon}_{xx} = A\tau_{xx}^n \\ &= A\tau_y^n, \end{aligned} \quad (\text{S7})$$

54 where flow law exponent  $n = 3$  and  $A$  is the flow rate parameter of Glen's flow law.

We integrate equation (S4) in  $x$  to find

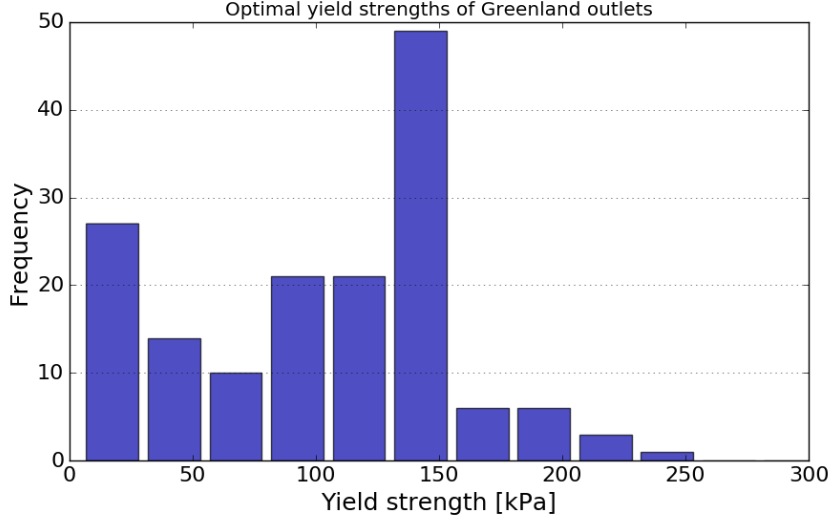
$$\int_0^L \frac{\partial H}{\partial t} dx + (HU)|_{x=L} = \int_0^L \dot{a} dx \quad (\text{S8})$$

$$U(x=L) = \frac{1}{H_{\text{terminus}}} \int_0^L \left[ \dot{a} - \frac{\partial H}{\partial t} \right] dx, \quad (\text{S9})$$

and by the chain rule  $\frac{\partial H}{\partial t} = \frac{\partial H}{\partial L} \frac{dL}{dt}$ . Separating the integral in equation (S9) and expanding  $\frac{\partial H}{\partial t}$  gives

$$U(x=L) = \frac{\dot{\alpha}L}{H_{\text{terminus}}} - \frac{dL}{dt} \frac{1}{H_{\text{terminus}}} \int_0^L \frac{\partial H}{\partial L} dx, \quad (\text{S10})$$

55 where  $\dot{\alpha} = \frac{1}{L} \int_0^L \dot{a} dx$  is the spatially-averaged ice accumulation rate along the flowline.



68

**Figure S2.** Histogram of optimal yield strength value found for each glacier.

We now substitute our expressions (S7, S10) in to equation (S4) and rearrange to find

$$\frac{dL}{dt} = \frac{\dot{a} - A\tau_y^3 H_{\text{terminus}} + \frac{\dot{\alpha}L}{H_{\text{terminus}}} \frac{\partial H}{\partial x}}{\frac{\partial H_y}{\partial x} - \frac{\partial H}{\partial x} \left(1 - \frac{1}{H_{\text{terminus}}} \int_0^L \frac{\partial H}{\partial L}\right)}. \quad (\text{S11})$$

56

We implement a discretized version of Equation S11 to describe the time evolution of glacier terminus position in SERMeQ.

57

### Text S3. The role of adjustable parameters

58

#### Yield strength $\tau_y$

59

For each glacier, we optimize the yield strength  $\tau_y$  to find the best fit between a reconstructed and observed centerline surface elevation profile. Glaciers with flatter surface slopes, including those close to flotation, are best fit by lower values of  $\tau_y$ . Steeper surface slopes are better fit by higher values of the yield strength. The optimization procedure is discussed in more detail in Ultee and Bassis (2016). The optimal value of  $\tau_y$  found for each glacier is listed in Supplementary Table 1. There is no correlation between optimal yield strength and glacier latitude, and no other spatial pattern is evident.

67

Figure S2 shows a histogram of the best-fit values of  $\tau_y$  obtained for the Greenland outlets we simulated. A central peak in the distribution shows that approximately 1/3 of the glaciers we simulate have an optimal yield strength between 125 kPa and 150 kPa. A smaller peak shows that there are also several glaciers in our set best fit by yield strengths between 5 kPa-25 kPa.

69

70

71

72

73

In this work, we have used a single value of  $\tau_y$  at both the ice-bed interface and the calving front. It is plausible that the ice-bed interface could be deforming more readily than the pure ice at the calving front, for example if the glacier bed is composed of saturated marine sediments or if the ice is very close to flotation. Such a case would lead to low ice surface slopes and a low optimal value of  $\tau_y$ , even though

74

75

76

77

78

79 pure ice throughout the glacier may be stronger. We discuss the case of  $\tau_{\text{bed}} < \tau_{\text{ice}}$  in  
80 Bassis and Ultee (2019).

### 81 **Ice temperature $T$**

82 The ice temperature  $T$  is used to select an appropriate value of the flow-rate  
83 parameter  $A$  in Glen’s flow law. Here, we use an ice temperature constant in space  
84 and time and do not optimize for its value. In our previous work, we have found that  
85 warmer ice ( $T = -2^\circ \text{C}$ ) is softer, forms smaller ice cliffs, and is more prone to rapid  
86 retreat. Conversely, colder ice ( $T = -30^\circ \text{C}$ ) is stiffer, able to form taller terminal  
87 ice cliffs, and retreats more slowly. For more details, we refer the interested reader to  
88 Ultee (2018).

### 89 **Text S4. Inclusion of submarine melt**

90 We do not explicitly simulate loss of ice from glacier termini by submarine melt-  
91 ing. Rather, we have constructed an upper-bound estimate of retreat that is consistent  
92 with high submarine melt rates. Our requirement that effective stress near the glacier  
93 terminus must equal the yield strength of ice (see Text S1) makes an implicit constraint  
94 on the submarine melt rate, because the rate of submarine melt shapes the stress field  
95 near glacier termini (Ma, 2018; Ma & Bassis, 2019). There are three cases to consider:

96 **Case I** The submarine melt rate is very small compared with the terminus velocity,  
97  $u_s \ll u_t$ . In this case, the terminus would be able to advance and thin episod-  
98 ically. However, advance and thinning would lower the effective stress at the  
99 glacier terminus, such that it would fall below the yield strength of ice and no  
100 longer satisfy our criterion. We therefore disallow Case I.

101 **Case II** The submarine melt rate is comparable to the terminus velocity,  $u_s \sim u_t$ . In  
102 this case submarine melt would balance the tendency of ice near the terminus to  
103 stretch and thin, maintaining the terminus ice thickness at the yield thickness.

104 **Case III** The submarine melt rate is very large compared with the terminus velocity,  
105  $u_s \gg u_t$ . In this case, the erosion of the terminus by high submarine melt would  
106 create an overhang and promote calving (Ma & Bassis, 2019). Considered at  
107 long enough time scales, e.g. the 0.25 annum standard time step in SERMeQ  
108 rather than the hours to days considered in finer-scale process models, high  
109 submarine melting and enhanced calving would also maintain the terminus ice  
110 thickness at the yield thickness.

111 Both Cases II and III are consistent with our assumption that there is a yielding  
112 boundary layer at the glacier front that constrains the terminus ice thickness (see  
113 Bassis & Ultee, 2019). The maximum rate of length change computed in Equation 1 is  
114 compatible with both cases, and the ice mass lost in each time step can be considered  
115 a combination of mass lost to calving and to submarine melting.

116 The upper-bound retreat rate that we have sought in this work does not require  
117 explicit simulation of the submarine melt rate. Nevertheless, future adaptations of  
118 our method to simulate calving in larger-scale models may seek to add a mechanism  
119 for forcing by time-varying submarine melt. We suggest that those efforts begin by  
120 allowing submarine melt rate  $u_s$  to modify the terminus velocity,  $U$  in Equation 1,  
121 with the understanding that doing so may introduce scenarios that are incompatible  
122 with our original assumptions.

## 123 **Text S5. Detailed case studies**

124 As described in the main article text, 40% of terminus positions simulated by  
 125 SERMeQ fall within the range of observed terminus position for the same year. Be-  
 126 cause SERMeQ is sensitive to bed topography features (Ultee, 2018) and is forced by  
 127 climate reanalysis data, model performance will generally be best where those data  
 128 products are most accurate. The agreement between modelled and observed retreat  
 129 of Sermeq Kujalleq (glacier ID 3, also called Jakobshavn Isbræ, main text Figure 3c),  
 130 where bed topography has been especially well examined by previous glaciological  
 131 studies, illustrates this point.

132 It is our aim to produce an upper bound on outlet glacier retreat and associated  
 133 mass loss. We demonstrated in Bassis and Ultee (2019) that Equation 1 is a theoretical  
 134 bound on the rate of calving retreat. Thus, we anticipate that the rate of retreat  
 135 simulated by SERMeQ will generally exceed the observed rate of retreat. To support  
 136 future implementation of this calving-rate bound in our model or others, it is important  
 137 to understand where it does not perform as expected. There are two cases to consider:  
 138 (1) the retreat rate simulated by SERMeQ is slower than the rate observed, or (2) the  
 139 retreat rate simulated by SERMeQ far exceeds the rate observed (by a factor of 5 or  
 140 more). We describe three illustrative examples here.

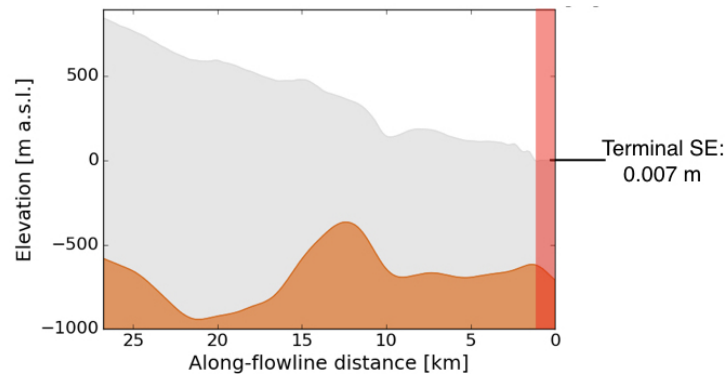
### 141 **Mean simulated retreat slower than observed**

142 Main text Figure 3b shows the simulated and observed changes in length for  
 143 Apuseeq Anittangasikkaajuk (MEaSURES Glacier ID 137), a small outlet glacier on  
 144 the east coast of Greenland. Our analysis shows that the mean rate of simulated  
 145 (single point) terminus retreat was 31 m/a, while the mean observed rate of retreat  
 146 of the terminus centroid was 87 m/a. This is one of only a handful of cases in which  
 147 the mean observed rate over the 2006-2014 period exceeds the supposed upper-bound  
 148 rate produced by Equation 1. However, in this case both rates are small, and the  
 149 simulated terminus position remains within the observed range of terminus positions.  
 150 We also note that Apuseeq Anittangasikkaajuk is seldom included in other studies of  
 151 Greenland outlets; as such, the quality of bed topography and climate data for this  
 152 outlet may be relatively lower.

### 153 **Mean simulated rate far exceeds observed**

154 Main text Figure 3d shows the simulated and observed changes in length for Hel-  
 155 heim Glacier (MEaSURES Glacier ID 175), a large and well-studied outlet in southeast  
 156 Greenland. The data quality for this outlet should be comparatively high. Neverthe-  
 157 less, SERMeQ simulates a mean retreat rate of 1980 m/a, which far exceeds the mean  
 158 observed retreat rate of 313 m/a. We attribute this rapid retreat to features in the  
 159 bed topography, combined with the no-flotation condition we have implemented in  
 160 SERMeQ.

161 The terminus of Helheim Glacier has been observed to float in some years, and  
 162 was likely floating at the beginning of our simulation period according to bed and  
 163 surface topography from Morlighem et al. (2017). The glacier bed is more than 600  
 164 m below sea level and retrograde for several kilometers upstream of the present ter-  
 165 minus, as shown in Figure S3. As explained in main text section 2 and in Ultee and  
 166 Bassis (2016, 2017), SERMeQ does not allow floating ice tongues to form. Where  
 167 small tongues are present, we remove them and simulate the first grounded point as  
 168 the “terminus”. In the case of Helheim Glacier, when we removed floating ice, the  
 169 simulated terminus was pushed onto the retrograde bed, where it began an unstable  
 170 retreat. In summary, the true near-terminus dynamics and stress field of Helheim  
 171 Glacier are shaped by the presence of floating ice that interacts with the fjord walls.



174 **Figure S3.** Near-terminus bed topography of Helheim Glacier. Brown filled region shows  
 175 glacier bed and grey filled region shows glacier ice, both from Morlighem et al. (2017). Note 10:1  
 176 exaggeration in vertical scale. A red overlay indicates floating ice that was removed in our simu-  
 177 lation. Annotation at figure left indicates the ice surface elevation at the terminus as recorded in  
 178 Morlighem et al. (2017), further evidence that the initial terminus could not have been grounded  
 179 ice.

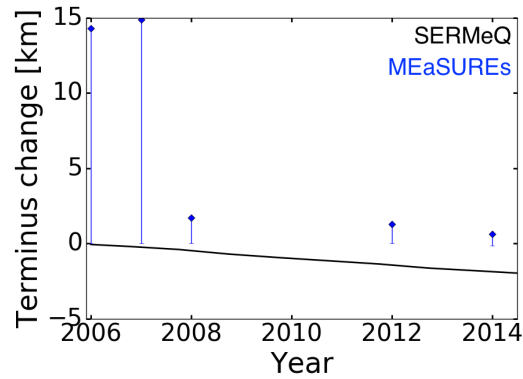
172 SERMeQ does not include these dynamics and therefore simulates an upper-bound  
 173 retreat that could occur in the absence of floating ice.

### 180 Successive under- and over-estimates within observed period

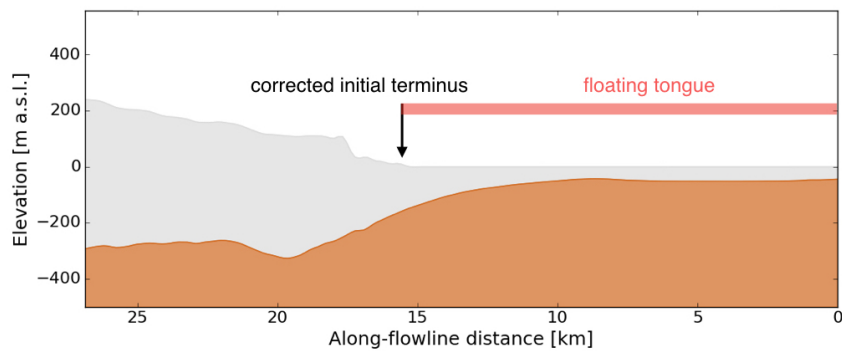
181 In a handful of other cases, the rate of retreat observed during a short period  
 182 exceeds the rate simulated during the same period. Underestimated retreat in one time  
 183 period is nearly always coupled with overestimated retreat in another period, such  
 184 that the aggregate effect over the course of the simulation remains an upper-bound  
 185 estimate of net retreat. For example, between 2007 and 2008, the floating ice tongue of  
 186 Hagen Brae (MEaSURES Glacier ID 105) disintegrated. The resulting observed rate of  
 187 retreat, more than 10 km/a, far exceeded the rate simulated by SERMeQ ( $< 1$  km/a)  
 188 over the same period (Figure S4). However, our model initialization had already  
 189 removed the floating portion of the glacier as of 2006, so the SERMeQ-simulated  
 190 terminus position was still more retreated than the observed. In the subsequent period  
 191 between 2008 and 2012, SERMeQ slightly overestimated the observed retreat rate.  
 192 Figure S4 illustrates this history. In Figure S5, we have annotated the floating ice  
 193 removed upon initialization, the collapse of which was responsible for anomalously  
 194 high observed retreat between 2007 and 2008.

### 207 References

- 208 Balmforth, N. J., Craster, R. V., Rust, A. C., & Sassi, R. (2006). Viscoplastic flow  
 209 over an inclined surface. *Journal of Non-Newtonian Fluid Mechanics*, 139(1–  
 210 2), 103 - 127. doi: 10.1016/j.jnnfm.2006.07.010
- 211 Bassis, J. N., & Ultee, L. (2019). A thin film viscoplastic theory for calving glaciers:  
 212 Towards a bound on the calving rate of glaciers. *Journal of Geophysical Re-*  
 213 *search: Earth Surface*, 124. doi: 10.1029/2019JF005160
- 214 Ma, Y. (2018). *Calving behavior of tidewater glaciers* (Doc-  
 215 toral dissertation, University of Michigan). Retrieved from  
 216 <https://deepblue.lib.umich.edu/handle/2027.42/146058>



195 **Figure S4.** Observed and simulated change in terminus position on Hagen Brae (glacier ID  
 196 105). Black curves indicate SERMeQ-simulated terminus positions, while blue markers indicate  
 197 MEaSUREs observations. The blue lines show the most-advanced and most-retreated parts of the  
 198 terminus projected onto the centerline, and blue diamonds indicate the centroid of the observed  
 199 terminus projected onto the centerline. Positive y-axis values indicate terminus positions more  
 200 advanced than the initial position; negative y-axis values indicate terminus positions retreated  
 201 from the initial position.



202 **Figure S5.** Near-terminus bed topography of Hagen Brae (glacier ID 105). Brown filled re-  
 203 gion shows glacier bed and grey filled region shows glacier ice, both from Morlighem et al. (2017).  
 204 Note 10:1 exaggeration in vertical scale. A red bar shows the length of floating ice that was re-  
 205 moved during our model initialization, and a black arrow indicates the first grounded point where  
 206 SERMeQ could establish an initial terminus.

- 217 Ma, Y., & Bassis, J. N. (2019). The effect of submarine melting on calving from  
218 marine terminating glaciers. *Journal of Geophysical Research: Earth Surface*,  
219 *124*(2), 334–346. doi: 10.1029/2018JF004820
- 220 Morlighem, M., Williams, C. N., Rignot, E., An, L., Arndt, J. E., Bamber, J. L., . . .  
221 Zinglensen, K. B. (2017). BedMachine v3: Complete bed topography and ocean  
222 bathymetry mapping of Greenland from multibeam echo sounding combined  
223 with mass conservation. *Geophysical Research Letters*, *44*(21), 11,051–11,061.  
224 doi: 10.1002/2017GL074954
- 225 Nye, J. F. (1951). The flow of glaciers and ice-sheets as a problem in plasticity.  
226 *Proceedings of the Royal Society of London A: Mathematical, Physical and*  
227 *Engineering Sciences*, *207*(1091), 554–572. doi: 10.1098/rspa.1951.0140
- 228 Ultee, L. (2018). *Constraints on the dynamic contribution to*  
229 *21st-century sea level rise from Greenland outlet glaciers* (Doc-  
230 toral dissertation, University of Michigan). Retrieved from  
231 <https://deepblue.lib.umich.edu/handle/2027.42/145794>
- 232 Ultee, L., & Bassis, J. N. (2016). The future is Nye: An extension of the perfect  
233 plastic approximation to tidewater glaciers. *Journal of Glaciology*, 1–10. doi:  
234 10.1017/jog.2016.108
- 235 Ultee, L., & Bassis, J. N. (2017). A plastic network approach to model calv-  
236 ing glacier advance and retreat. *Frontiers in Earth Science*, *5*(24). doi:  
237 10.3389/feart.2017.00024